Arab J Geosci
DOI 10.1007/s12517-013-0974-6

ORIGINAL PAPER

A spatial statistical analysis of the occurrence of earthquakes along the Red Sea floor spreading: clusters of seismicity

Khalid Al-Ahmadi · Abdullah Al-Amri · Linda See

Received: 28 January 2013 / Accepted: 17 May 2013

Abstract The aim of this study is to apply spatial pattern analysis techniques to a seismic data catalog of earthquakes beneath the Red Sea to try and detect clusters and explore global and local spatial patterns in the occurrence of earthquakes over the years from 1900 to 2009 using a geographical information system (GIS). The spatial pattern analysis techniques chosen for this study were quadrant count analysis, average nearest neighbor, global Moran's I, Getis–Ord general G, Anselin Local Moran's I, Getis–Ord Gi*, kernel density estimation, and geographical distributions. Each of these techniques was implemented in the GIS so that computations could be carried out quickly and efficiently. Results showed that (1) these techniques were capable of detecting clusters in the spatial patterns of the occurrence of the earthquakes; (2) both global and local spatial statistics indicate that earthquakes were clustered in the study area beneath the Red Sea; (3) earthquakes with higher magnitudes on the Richter scale were notably concentrated in the central and southern parts of the Red Sea where seismic activities were most active; and (4) earthquakes with moderate magnitudes on the Richter scale were particularly concentrated in the northern part of the Red Sea where there is an area of late-stage continental rifting comprised of a broad trough without a recognizable spreading center, although there were several small, isolated deep troughs. We conclude that the pattern analysis techniques applied to the seismic data catalog of earthquakes beneath the Red Sea could detect clusters in the occurrence of earthquakes from 1900 to 2009.

Keywords Earthquakes · Clusters · Spatial pattern analysis · Spatial statistics · GIS · Red Sea

K. Al-Ahmadi (✉)
King Abdulaziz City for Science and Technology,
Riyadh, Saudi Arabia
e-mail: alahmadi@kacst.edu.sa

A. Al-Amri
King Saud University, Riyadh, Saudi Arabia

L. See
International Institute for Applied Systems Analysis,
Laxenburg, Austria

L. See
Centre for Advanced Spatial Analysis, University College London,
London, UK

Introduction

The Red Sea formed during the Eocene–Oligocene period and is one of the world's youngest oceanic basins (Al-Amri 1995). The boundary between the African and Arabian continental plates follows the principal axis and runs along the entire length of the sea floor (Fig. 1). As the two continental plates are slowly moving apart, the land beneath the Red Sea falls within an active seismic area and experiences frequent earthquakes. The Red Sea is a typical oceanic rift dating back to 5.7 Ma ago (Roeser 1975) and was one of the first areas to be interpreted in the framework of plate tectonics (McKenzie et al. 1970). It is a divergent-type boundary between the African and Arabian plates and is a NNW–SSE trending depression (El-Shazly 1982; Hamouda 2009).

The Red Sea area has experienced several major earthquakes in the past. In 1121, an earthquake occurred along the main trough with a magnitude of 6.9 that was felt over a wide area and caused damage to structures located 300 km apart such as Madinah and Makkah (Ambraseys et al. 1995). Between 1884 and 1980, 24 earthquakes with magnitudes between 6 and 6.9 struck the Red Sea. On 31 March 1969, an earthquake of magnitude 6.9 occurred at the Gulf of Suez (Abdel-Rahman et al. 2009) while on 13 December 1982, the highlands of Dhamar in Yemen (160 km to the Red Sea) were hit with an earthquake of magnitude 6.0, killing 2,800 people, injuring a further 1,500, and leaving around 400,000 people homeless (Choy and Kind 1987). The largest event of moment

Published online: 04 June 2013

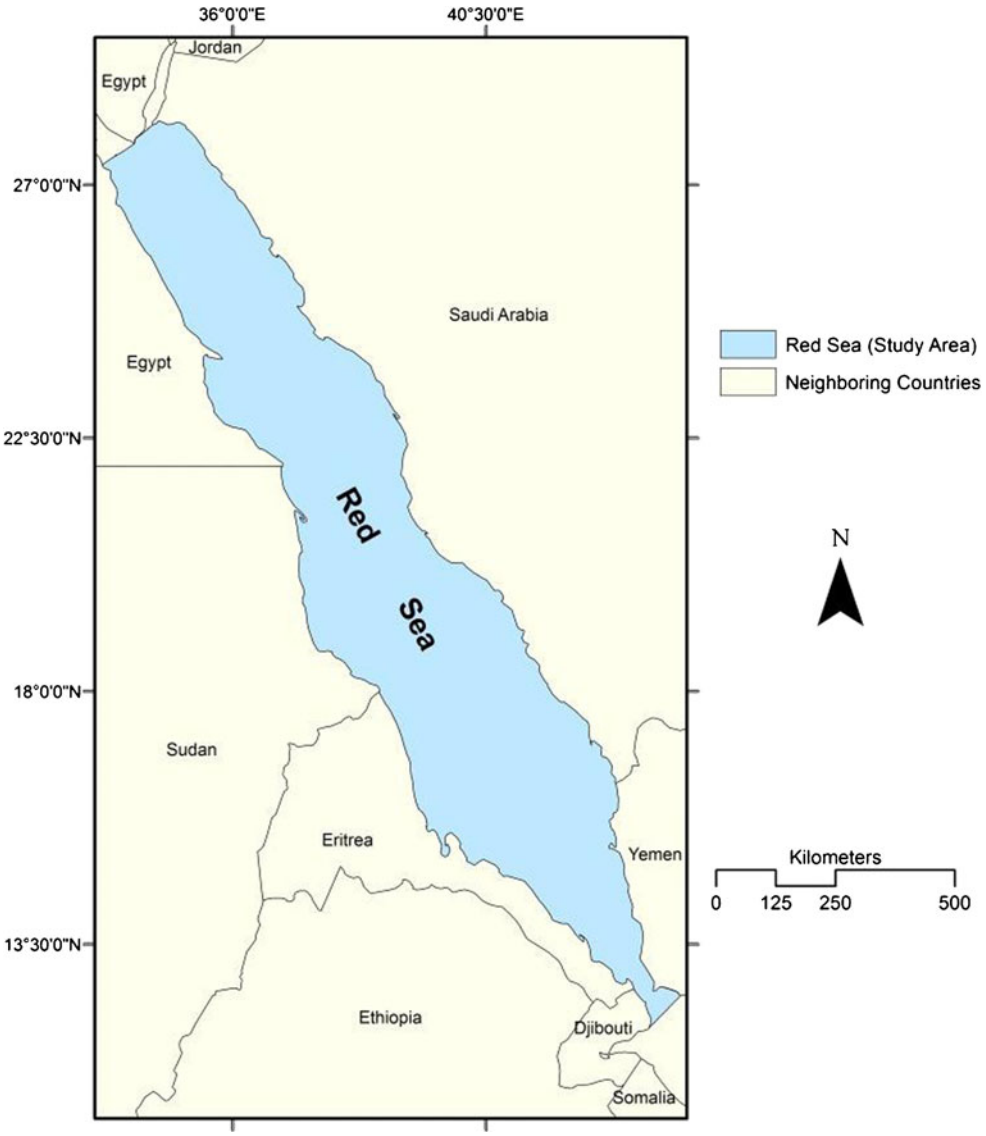

Fig. 1 Location map of the study area showing the tectonic setting. The Red Sea floor spreading represents the plate boundary between Arabian and African plates

magnitude (M_w) 7.1 took place on 22 November 1995 at the Gulf of Aqaba, causing structural damage to buildings in several cities along the gulf coast (Al-Tarazi 2000).

The Red Sea can be tectonically classified into three distinct zones according to the geophysical and morphological features that demonstrate diverse stages in the evolution of the rift. These zones comprise a southern section (15–20° N) in which active seafloor spreading is occurring and demonstrates a well-defined and continuous axial trough, an intermediate transition zone (20–23.5° N), which is covered with distant cells of seafloor spreading and a series of large deep features with frequent metalliferous deposits. The northern zone (23.5–28° N) is a section with a number of minor dips and is characterized by the presence of an axial depression, which is presently in the late stages of continental rifting and is expected to be underlain by thinned, stretched continental crust near breaking point, more or less intruded by basic bodies (Cochran 1983; Cochran et al. 1985, 1986; Pautot et al. 1986; Bonatti 1985).

Al-Amri (1995) studied the recent seismicity and swarm activity in the northern Red Sea with regard to the tectonics and structures identified by surface geology and marine magnetic anomalies. It was noted that seismicity activity seemed to be low compared to the remaining part of the Red Sea. The study confirmed that the comparatively low level of seismicity in the northern Red Sea should not reduce the likelihood of more significant seismic events since such swarms may release energy that could cause larger events in the future. Al-Amri et al. (1998) examined the spatial distribution of the seismicity parameters in the Red Sea regions. They observed that the likely occurrence of major earthquakes is distributed over a wide area categorized by the presence of rift zones, structural discontinuities, and dislocations. Korrat et al. (2006) analyzed the seismicity in the northernmost part of the Red

Sea and defined three earthquake zones affecting the area and suggested that the thermal activity and the triple junction nature control the activity in this area.

One approach to understanding patterns in the occurrences of earthquakes in a chosen geographical area has been to apply point pattern analysis to the stochastic process that has resulted in the observed point pattern. This type of analysis is then used to determine whether or not these events are regularly spaced or clustered in space and time. Vere-Jones (1970) was one of the pioneers who applied stochastic models to study the occurrence of earthquakes in New Zealand. Several scientists have contributed papers in which similar models were applied to data about earthquakes from different historical catalogs and in many different parts of the world (Vere-Jones and Deng 1988; Ogata 1988; Musmeci and Vere-Jones 1992; Shurygin 1993; Holden et al. 2003; Faenza et al. 2004; Pei et al. 2007; Vasudevan et al. 2007; Han et al. 2008; Zimeras 2008; Pei et al. 2009; Pei 2011). From reviewing the scientific literature, there is further scope for investigating to what extent one could detect clusters of earthquakes and analyze spatial distributions of these clusters in relation to geological, tectonic, or seismic activities which may be significant for modeling the occurrence of earthquakes as a point process. Thus, the aim of this research is to apply a range of different spatial pattern analysis techniques beyond those used previously in the study of earthquakes. These techniques are used to search for clusters and explore the global and local spatial patterns in the occurrence of earthquakes in the Red Sea for the period 1900–2009.

Seismic data and methods

Seismic data catalog and processing of data

Seismic data for the Red Sea area were acquired from the Seismic Studies Center at King Saud University (KSU), King Abdulaziz City for Science and Technology (KACST), and Saudi Geological Survey (SGS). The KSU database covered the period up to 2003, the KACST database contained events from 2004 to 2005 while the SGS contained data from 2006 to 2009. In addition, the earthquake data were available from the Egyptian National Seismological Network bulletins (1997–2009). Historical data have been collected from Ambraseys et al. (1995). International data centers have been searched for additional data such as the International Seismological Center for the period from 1964 to 1998, and the National Earthquake Information Center as well. All of the data were then combined into a single database and sorted by source, which allowed for quality checking, e.g., historical cross-checking and removal of incorrect or duplicated records.

The compiled catalog includes the recoded earthquakes in the range of $1 \leq m \leq 7.5$ of different magnitude scales covering the time interval from 1900 to 2009. For the homogeneity of this catalog, all magnitudes scales have been converted into unified magnitude scale as M_w as the moment magnitude is the most reliable and worldwide magnitude scale. Aftershocks, foreshocks, and swarm type activities have been removed from the compiled catalog using the approach of Gardner and Knopo (1974). The seismic and other spatial data were then processed and a spatial statistical analysis was conducted using a geographical information system (GIS; ESRI ArcGIS 10.1). Figure 2 shows the spatial distribution of the earthquakes during 1900–2009 in the study area. The density of earthquakes was estimated using a kernel function in the GIS to fit a smoothly tapered surface to the location of each earthquake using the magnitude as a weight.

Spatial statistical analysis

Point pattern analyses typically begin with a test for complete spatial randomness where the null hypothesis states that the pattern is random. This test enables one to differentiate between patterns which are of no further interest (i.e., random) and those which may be of interest. Regularly spaced patterns or those exhibiting aggregated patterns or clusters (Diggle 2003), when we apply quadrat count analysis and the average nearest neighbor index, are of interest. Other statistical methods can be used to summarize the pattern and/or trend over the extent of the study area. These statistical methods can be categorized into global and local.

Global statistics generally yield only one metric which provides a summary of the pattern and/or trend over the whole of the study area. The application of global statistics relies on a set of basic assumptions, e.g., homogeneity across the study area and the independence of the observations (Páez 2004). If these assumptions do not hold, however, then the use of a single metric is inappropriate (Anselin 1995, 2005; Fotheringham et al. 2002). This is particularly true in the case of spatial data where the effects of spatial autocorrelation are common (Anselin 1995).

On the other hand, local statistics identify spatial variation in the relationships between variables, in particular for identifying the presence of clusters or hot spots, for testing for assumptions of heterogeneity and for determining the distance beyond which spatial effects between variables cease (Anselin 1995; Getis and Ord 1992). Global and local statistics can be used in a complementary fashion to achieve a thorough understanding of spatial patterns and processes. The first four statistics considered in this paper are global: (1) quadrant count analysis, (2) average nearest neighbor, (3) global Moran's I, and (4) Getis–Ord general G. The second three statistics are local: (1) Anselin local Moran's I, (2) Getis–Ord Gi*, and (3) kernel density estimator are local statistics. Additionally, four methods were applied to analyze the geographic distribution of earthquakes including: directional distribution, central feature, mean center,

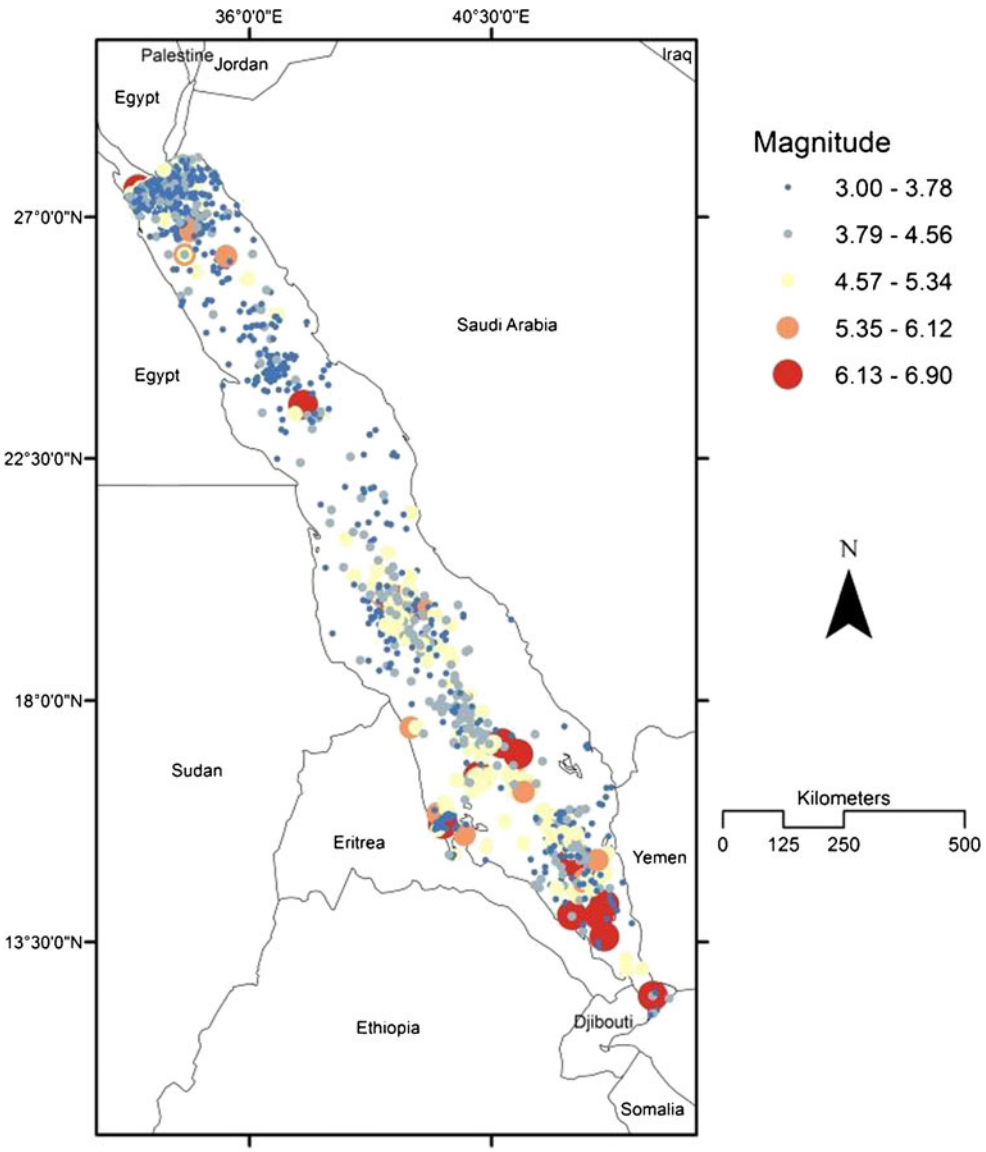

Fig. 2 Distribution of the earthquakes during 1900–2009 in the study area

and median center. These different methods are described briefly in the sections that follow.

Quadrat count analysis

Quadrat count analysis (QCA) involves partitioning the region into an equal set of subregions referred as quadrats. The frequency distribution of the number of points per quadrat is then calculated and the variance-to-mean ratio (VTMR) or the index of dispersion is used to evaluate the pattern:

$$\mathrm{VTMR} = \frac{\sigma^2}{\mu} \tag{1}$$

where σ^2 is the variance and μ is the mean. If the VTMR is greater than 1, the pattern is clustered, if the VTMR equals 1, then the pattern is random and if it is less than 1, the pattern is regular. Note that the resolution of the quadrat can influence the results, e.g., if the quadrat size is too small, then each quadrat may contain too few events to pick up a pattern while too large a quadrat may only pick up a coarse description of the pattern. A rule of thumb is that the quadrat size is twice the expected frequency of points in the study area although trial and error can be used to select the best quadrat size. However, QCA does not take the proximity of features into account, which is the case with other spatial statistics such as the nearest neighbor as described below (Mitchell 2005; Kalkhan 2011).

Average nearest neighbor

The average nearest neighbor (ANN) computes a nearest neighbor index based on the average Euclidean distance from

each feature to its nearest neighboring feature:

$$\mathrm{ANN} = \frac{\overline{D}_O}{\overline{D}_E} \tag{2}$$

where $\overline{D}_O$ is the observed mean distance between each feature and its nearest neighbor:

$$\overline{D}_O = \frac{\Sigma_{i=1}^{n} d_i}{n} \tag{3}$$

where d_i equals the distance between feature i and its nearest neighbor, n corresponds to the total number of features, A is the total study area and $\overline{D}_E$ is the expected average distance between features given a hypothetical random pattern:

$$\overline{D}_E = \frac{0.5}{\sqrt{n/A}} \tag{4}$$

The ANN computes a nearest neighbor index based on the average distance from each feature to its nearest neighboring feature (x and y coordinates only) and the associated z values. If the index is less than 1, the pattern indicates clustering. If an index is more than 1, the pattern exhibits a tendency towards dispersion. Z scores, or measures of standard deviation, indicate the statistical significance. If a Z score was less than −1.96 or greater than 1.96 in the analysis, the pattern exhibits significant clustering or dispersion respectively ($p<0.05$). If the Z score was between 1.96 and −1.96, the pattern exhibits a random distribution (Mitchell 2005; Kim et al. 2012).

Global Moran's I

The global Moran's I (GMI) statistic provides a measure of the degree of spatial autocorrelation based on both the locations of events and the values associated with the events at the same time. The GMI statistic indicates the degree of spatial concentration or dispersion for a given point pattern (Scott and Janikas 2010). GMI and the associated Z values will be calculated to determine if the spatial pattern of earthquakes was clustered, dispersed or random. If the Z score is less than −1.96 or greater than 1.96 in the spatial autocorrelation analysis, the pattern exhibited dispersion or clustering, respectively ($p<0.05$). Z scores between −1.96 and 1.96 exhibit a random pattern (Mitchell 2005; Kim et al. 2012).

The GMI is calculated as follows:

$$\mathrm{GMI} = \frac{n}{S_o} \frac{\Sigma_{i=1}^{n} \Sigma_{j=1}^{n} \omega_{i,j} z_i z_j}{\Sigma_{i=1}^{n} z_i^2} \tag{5}$$

where Z_i is the deviation of an attribute for feature i from its mean $\left(x_i - \overline{X}\right)$, $\omega_{i,j}$ is the spatial weight between feature i and j, n is equal to the total number of features, and S_o is the aggregate of all of the spatial weights.

Getis–Ord general G

The Getis–Ord general G (GOGG) statistic was developed by Getis and Ord as a global statistic for analyzing spatial patterns (Getis and Ord 1992; Ord and Getis 1995). The GOGG quantifies the extent of clustering for either high or low values to find out whether either hot spots (clusters of high values) or cold spots (clusters of low values) exist in a study area. If the Z score value is positive, the observed GOGG is larger than the expected GOGG, indicating that high values for the attribute are clustered in the study area. If the Z score value is negative, the observed GOGG is smaller than the expected index, indicating that low values are clustered in the study area. The GOGG statistic of overall spatial association is calculated as follows:

$$\mathrm{GOGG} = \frac{\Sigma_{i=1}^{n} \Sigma_{j=1}^{n} \omega_{i,j} x_i x_j}{\Sigma_{i=1}^{n} \Sigma_{j=1}^{n} x_i x_j}, \forall_{j \neq i} \tag{6}$$

where x_i and x_j are attribute values for features i and j, and $\omega_{i,j}$ is the spatial weight between these two features.

Anselin local Moran's I

Anselin (1995) suggested a local Moran's I index of spatial association to identify local clusters and spatial outliers that can be calculated as follows:

$$I_i = \frac{x_i - \overline{X}}{S_i^2} \sum_{j=1, j \neq i}^{n} \omega_{i,j} \left(x_j - \overline{X}\right) \tag{7}$$

where x_i is an attribute for feature i, $\overline{X}$ is the mean of the corresponding attribute, and $\omega_{i,j}$ is the spatial weight between feature i and j. Positive values for the Anselin local Moran's I index indicate that a feature has neighboring features with similarly high or low attribute values; this feature is part of a cluster. Negative values for this index, on the other hand, indicate dissimilar values of neighboring features, which are considered to be an outlier. In both cases, the p value for the event must be small enough ($p<0.05$) for the cluster or outlier to be considered statistically significant.

*Getis–Ord Gi**

The Getis–Ord *Gi** statistic (Ord and Getis 1995; Getis and Ord 1992; Mitchell 2005) identifies statistically significant

Table 1 Descriptive statistics of earthquakes beneath the Red Sea

Magnitude (M)	Count of earthquakes	% of earthquakes	Minimum magnitude	Maximum magnitude	Mean magnitude	SD magnitude
3	171	9	3	3	3	0
$3<M\leq4$	1,164	62	3.04	4	3.43	0.28
$4<M\leq5$	434	23	4.09	5	4.50	0.28
$5<M\leq6$	97	5	5.10	6	5.33	0.23
$6<M\leq7$	22	1	6.1	6.9	6.4	0.27
$3\leq M\leq7$ (all)	1,888	100	3	6.9	3.77	0.72

hot spots and cold spots within the context of neighboring features and is calculated as follows (Mitchell 2005):

$$G_i^* = \frac{\Sigma_{j=1}^{n}\omega_{i,j}x_j - \overline{X}\Sigma_{j=1}^{n}\omega_{i,j}}{s\sqrt{\frac{\left[n\sum_{j=1}^{n}\omega_{i,j}^2 - \left(\sum_{j=1}^{n}\omega_{i,j}\right)^2\right]}{n-1}}} \quad (8)$$

where x_j is the attribute value for feature, j, and $\omega_{i,j}$ is the spatial weight between feature i and j for n features. Gi^* uses a neighborhood based either on adjacent features or on a set distance and returns a Z score. For statistically significant positive Z scores, the larger the Z score is, the more intense the clustering of high values (i.e., a hot spot). For statistically significant negative Z score, the smaller the Z score is, the more intense the clustering of low values (i.e., a cold spot). A Gi^* value near zero indicates the absence of clustering of either high or low values surrounding the target feature. This happens when the surrounding values are near the mean, or when the target feature is surrounded by a mix of high and low values.

Kernel density estimator

A kernel density estimator (KDE) is a nonparametric spatial interpolation method for analyzing the first-order properties of a point event distribution by computing event density (Silverman 1986; Bailey and Gatrell 1995; Xie and Yan 2008). The general form of the KDE in a two-dimensional space is given by:

$$\lambda(s) = \sum_{i=1}^{n}\frac{1}{\pi r^2}k\left(\frac{d_{is}}{r}\right) \quad (9)$$

where $\lambda(s)$ is the density at location s, r is the search radius or bandwidth of the KDE, n is the number of sampling points, and k is the weight of a point i at distance d_{is} to location s. The surface value is the peak at the location of the point and reduces with increasing distance from the point, reaching zero at the search radius distance from the point. The variable k is usually modeled as a kernel function of the ratio between d_{is} and r. KDE was applied in this study to generate a continuous surface map of earthquake density based on individual earthquake locations and magnitudes values, in which the density at each location reflects the concentration of earthquakes in the surrounding area. From this, it is possible to see how earthquakes densities vary across the Red Sea.

Directional distribution, central feature, mean center, and median center

Four methods will be used in this work to measure the geographic distribution of earthquakes including: directional distribution, central feature, mean center, and median center. The directional distribution (standard deviational ellipse) creates

Table 2 Quadrant count analysis (QCA)

Magnitude (M)	Quadrant Count Analysis			
	Average	Variance	VTMR	Pattern
3	0.61	3.90	6.38	Clustered
$3<M\leq4$	4.15	141.57	34.05	Clustered
$4<M\leq5$	1.55	18.08	11.66	Clustered
$5<M\leq6$	0.34	3.63	10.50	Clustered
$6<M\leq7$	0.07	0.13	1.65	Clustered
$3\leq M\leq7$ (all)	6.74	287.67	42.66	Clustered

Table 3 Average nearest neighbor (ANN)

Magnitude (M)	Average Nearest Neighbor			
	Index	z Statistic	p Value	Pattern
3	0.26	−18.34	0.00**	Clustered
$3<M\leq4$	0.30	−45.34	0.00**	Clustered
$4<M\leq5$	0.44	−22.023	0.00**	Clustered
$5<M\leq6$	0.47	−9.90	0.00**	Clustered
$6<M\leq7$	0.899	−0.90	0.36	Random
$3\leq M\leq7$ (all)	0.34	−54.56	0.00**	Clustered

Table 4 Global Moran's I (GMI)

Magnitude (M)	Global Moran's I			
	Index	z Statistic	p Value	Pattern
3	–	–	–	–
$3<M\leq4$	0.04	16.10	0.00**	Clustered
$4<M\leq5$	0.07	9.03	0.00**	Clustered
$5<M\leq6$	0.008	1.02	0.30	Random
$6<M\leq7$	0.11	2.55	0.01*	Clustered
$3\leq M\leq7$ (all)	0.13	68.89	0.00**	Clustered

standard deviational ellipses to summarize the spatial characteristics of geographic features (earthquakes): central tendency, dispersion, and directional trends. The central feature identifies the most centrally located feature. The mean center identifies the geographic center (or the center of concentration) for a set of earthquakes. The median center measures the central tendency that is robust to outliers. It identifies the location that minimizes travel from it to all other features in the dataset (Mitchell 1999).

Results

Our earthquake catalog includes 1,888 earthquakes in the study area beneath the Red Sea from 1900 to 2009. The descriptive statistics are summarized in Table 1. The highest percentage of earthquakes had magnitudes between 3 and 4 (62 %) on the Richter scale. Magnitudes greater than 5 on the Richter scale occurred in 6 % of cases. The summary statistics indicate that the area is seismically active.

Global spatial statistics including QCA, ANN, GMI, and GOGG were applied to the earthquake dataset (Tables 2, 3, 4, and 5). For the QCA, the VTMR was 42.66 or greater than 1, which indicates a tendency towards clustering. The ANN, GMI, and GOGG values were 0.34, 0.13, and 0.11, respectively, where values of less than 1 indicate clustering. Thus, all four statistics indicate that the pattern of earthquake occurrence beneath the Red Sea from 1900 to 2009 was spatially clustered.

Table 5 Getis–Ord general G (GOGG)

Magnitude (M)	Getis–Ord general G			
	Index	z Statistic	p Value	Pattern
3	–	–	–	–
$3<M\leq4$	0.13	−2.61	0.008**	Low clusters
$4<M\leq5$	0.12	−1.03	0.30	Random
$5<M\leq6$	0.30	−1.16	0.24	Random
$6<M\leq7$	0.42	−1.75	0.07*	Low clusters
$3\leq M\leq7$ (all)	0.11	−5.45	0.00**	Low clusters

The global indices were then applied to each of the five earthquake magnitude categories shown in Table 1. The results of this analysis are in Tables 2, 3, 4, and 5. Only the results for QCA consistently indicate a tendency towards spatial clustering for all earthquake magnitudes. In contrast, the ANN and GMI results show clustering in all categories except in the largest cases of the ANN, i.e., $6<M\leq7$ and $5<M\leq6$ for the GMI, where the two indicators suggest a random occurrence of events for these specific categories. The GOGG showed low clustering for three categories and random for categories $4<M\leq5$ and $5<M\leq6$. Thus, the different global indices appear to give some conflicting results when compared with one another.

Since the QCA, ANN, GMI, and GOGG are global statistics, they yield only one metric which summarizes the pattern over the entire extent of the study area. KDE, Anselin local Moran's I, and Getis–Ord Gi*, which are local statistics, were therefore applied to the dataset because they may identify the presence and location of clusters or hot spots across the study region.

Figure 3a–f shows the hot spot patterns of earthquake occurrence based on KDE for the full dataset and varying categories of magnitude. The full dataset (Fig. 3a) shows the presence of a large cluster in the northern part of the Red Sea which is largely characterized by events of magnitude 5 and less (Fig. 3b–d), and clusters across the southern half of the Red Sea, which are characterized by higher magnitude events (Fig. 3d–f). Some smaller clusters can be seen in Fig. 3b in the northern half of the Red Sea which are not as pronounced when examining all magnitudes together (Fig. 3a). Thus, the KDE shows some distinctive clustering patterns for all magnitudes of earthquake occurrence.

Figure 4a–f show the results of analyzing directional distribution across different categories of magnitude in order to determine whether or not the seismic activity beneath the Red Sea area exhibited a directional trend. For this analysis, we applied 1 SD which uses approximately 68 % of earthquakes from each category in the analysis. The directional distribution is shown on the figures by the standard deviational ellipse. The results indicate that 68 % of earthquakes with a magnitude of 3 are located in the northern and central parts of the Red Sea while the highest magnitude events are concentrated in the central and southernmost sections. Figure 4a–f shows the location of the mean center, median center, and central feature of the earthquakes. These three measures indicate that earthquake occurrence shifts from north to south as the magnitude increases. These findings are similar to those found using KDE.

Figure 5a shows the locations of earthquakes with significant Anselin local Moran's I statistics, which were applied to identify significant clusters or spatial outliers using the degree

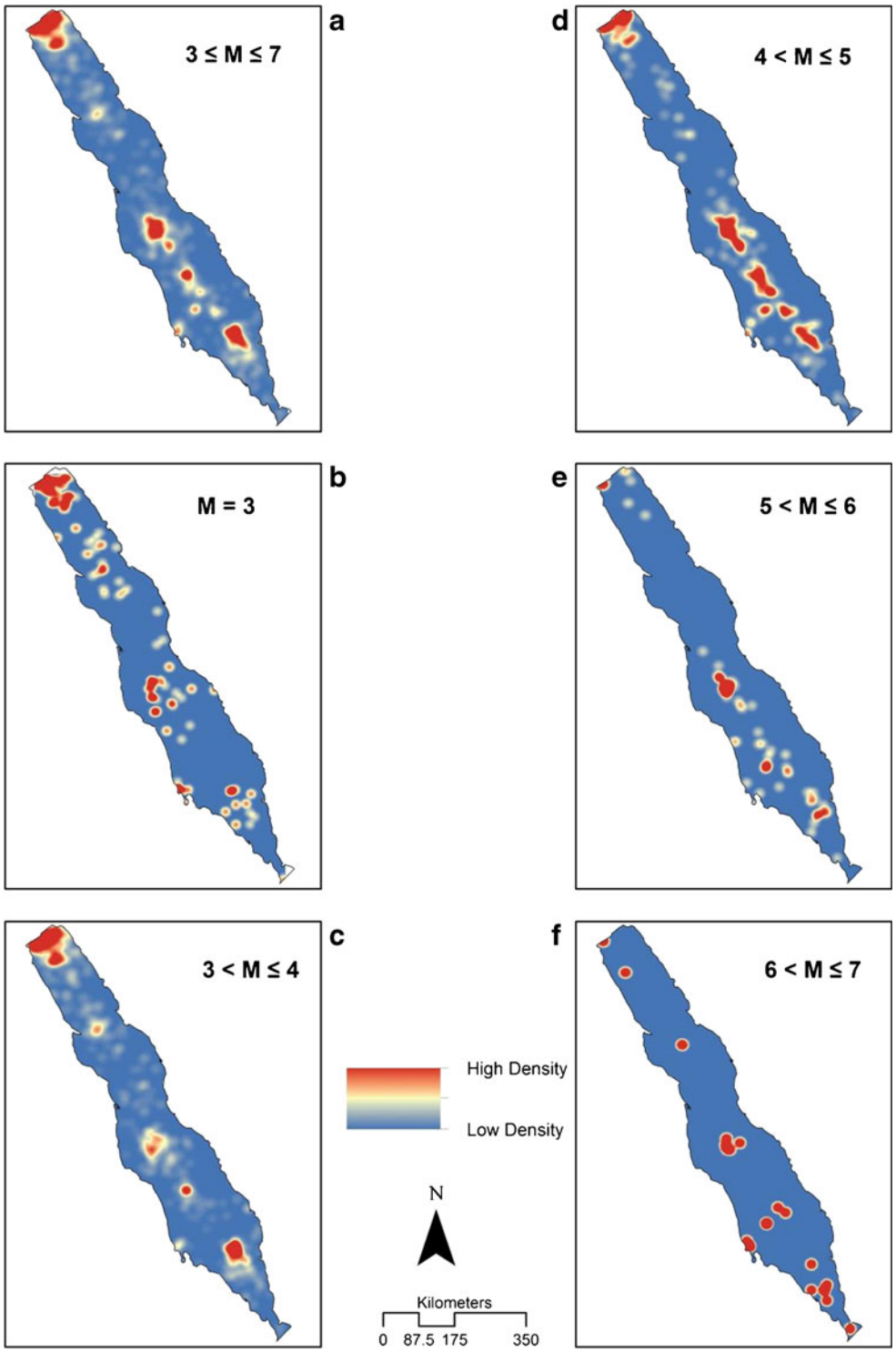

Fig. 3 Kernel density estimation (KDE) applied to the earthquake events for **a** all magnitudes and for earthquakes with the following magnitudes: **b** M=3, **c** 3<M≤4, **d** 4<M≤5, **e** 5<M≤6, **f** 6<M≤7

of spatial autocorrelation of earthquake occurrence weighted by magnitude of the event. Spatial clusters are indicated by dark red and dark blue dots. The dark red dots show earthquakes with high magnitudes which are surrounded by earthquakes with high magnitudes. In contrast, the dark blue dots indicate low magnitude earthquakes surrounded by other earthquakes of low magnitudes. The light red and light blue dots indicate the presence of spatial outliers, i.e., high magnitude events surrounded by low events and vice versa. There are clearly spatial clusters of earthquakes occurring in specific areas of the Red Sea. The results show similar patterns to those of the two previous local statistics, i.e., the earthquakes have a north–south distribution with lower magnitude events in the north and higher ones in the south. In particular, there are two clusters of

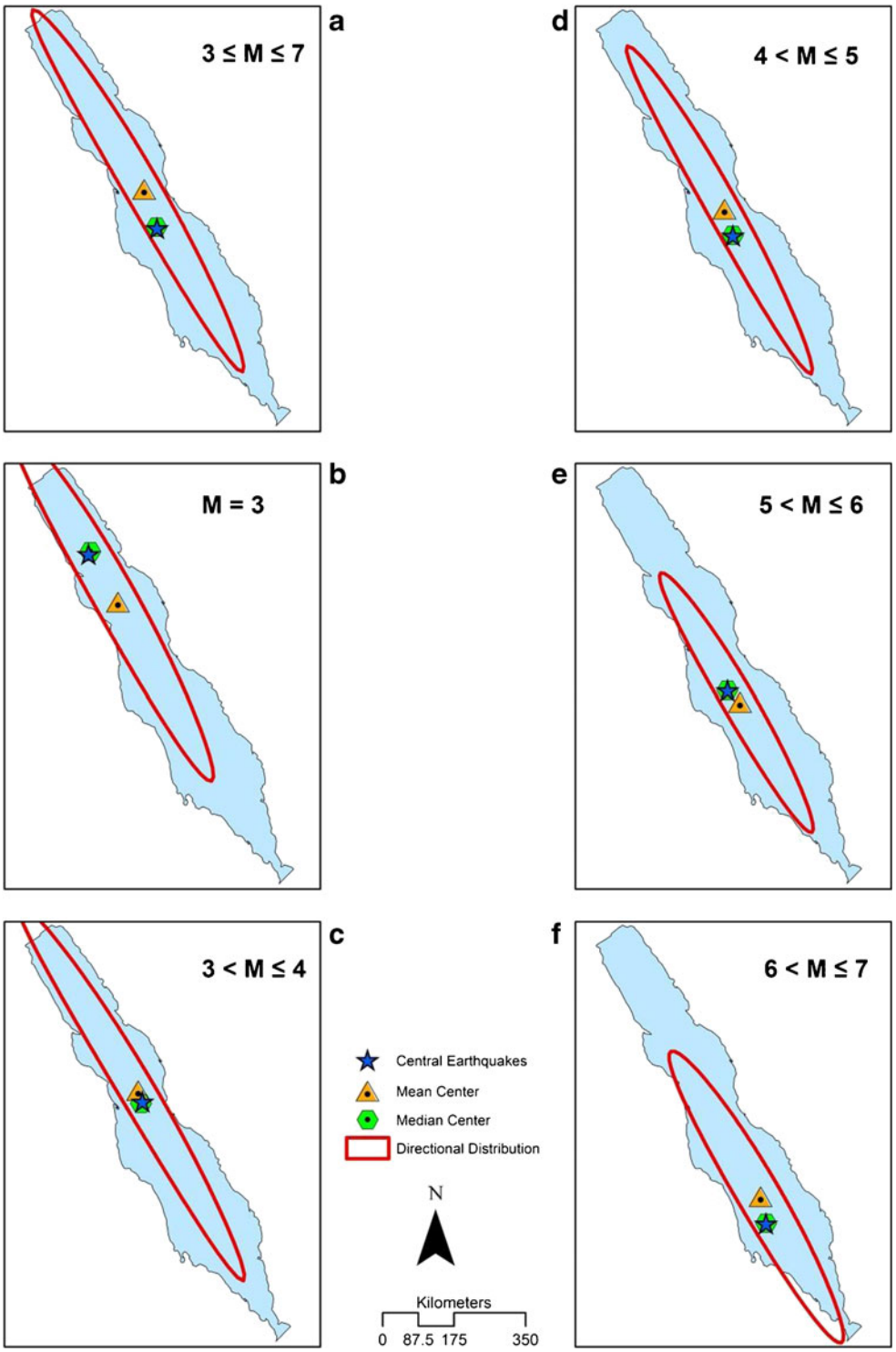

Fig. 4 Directional distribution, central feature, mean center and median center for earthquakes of **a** all magnitudes and for earthquakes with the following magnitudes **b** $M=3$, **c** $3<M\leq4$, **d** $4<M\leq5$, **e** $5<M\leq6$, **f** $6<M\leq7$

earthquakes with high magnitudes, one large cluster in the middle of the Red Sea (between 16 and 21° N) and another smaller one in the southern part (between 13 and 15° N).

There are also clusters of earthquakes with lower magnitudes. There is a medium-sized cluster at the northern end of the Red Sea (between 26 and 28° N), a smaller one in the northern part located between 23°45′ and 25°30′N, and the smallest cluster in the southern part between 15°10′ and 16°10′N. Other parts of the Red Sea exhibit random patterns of earthquake occurrence and distribution.

Figure 5b shows the location of earthquakes beneath the Red Sea with significant Getis–Ord Gi* statistics. The Getis–Ord Gi* identifies hot spots of earthquake occurrence. Hot spots can be characterized into four types:

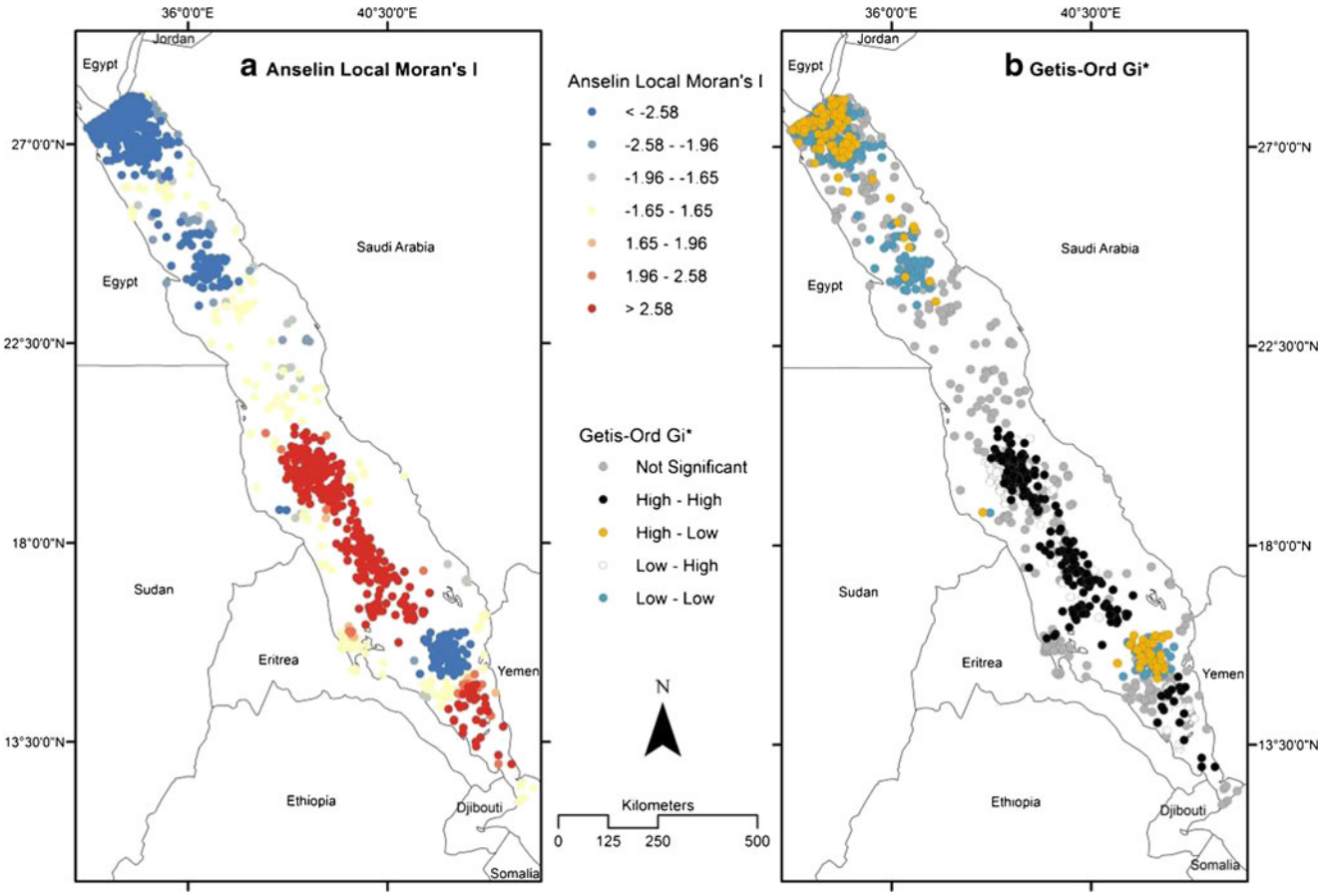

Fig. 5 **a** Cluster analysis using the Anselin local Moran's I and **b** hot spot analysis using Getis–Ord Gi*

high–high or hot spots, in which high magnitude events are surrounded by other high magnitude events; low–low or cold spots, where the same is true but the events are of a low magnitude; high–low, where high magnitude events are surrounded by low magnitude events; and low–high, which is the opposite of high–low. The black and blue dots in Fig. 5b indicate significant hot and cold spots, respectively. The Getis–Ord Gi* analysis suggests there are statistically significant hot spots in the middle of the Red Sea (between 16° and 20°30′N) and a very small cluster in the southern part (between 14°20′ and 14°50′N). The results also suggest a mixture between low–low clusters and high–low clusters at two locations beneath the Red Sea, one in the northern part of the Red Sea between 26° and 28° N and the other in the southern part between 15° and 16° N. Note that the clusters of low–low are larger than the high–low clusters in one of the two locations. There is only one small cold spot in the northern region of the Red Sea located between 23°50′ and 24°30′N.

Based on the results of applying the Anselin local Moran's I and the Getis–Ord Gi* statistics, earthquakes with moderate to high magnitudes are concentrated in areas located between 16°10′ and 20°30′N. This area can therefore be regarded as seismically active. The advantage of using Getis–Ord Gi* compared with the Anselin local Moran's I statistics is that the former provides more local details about the clusters. For example, the Anselin local Moran's I indicated that the northernmost part of the Red Sea can be categorized as having clusters of low magnitude earthquake events, while the Getis–Ord Gi* analysis showed further spatial disaggregation into low–low magnitudes clusters and high–low clusters. This provides greater certainty in terms of where hot spots are located, i.e., the most risky areas.

Discussion

The aims of this research were to detect clusters and to explore spatial patterns in the occurrence of earthquakes beneath the Red Sea from 1900 to 2009. A range of different global and local spatial statistical techniques were applied using a GIS.

Both global and local spatial statistics indicate that earthquakes are clustered beneath the Red Sea. Earthquakes with higher magnitudes on the Richter scale were concentrated notably in the central and southernmost parts of the Red Sea, the most active zone in terms of seismic activities. One reason for this clustering may be because this area is located in a zone of active sea-floor spreading, which is characterized by a well-developed, deep axial trough that has been produced through

normal seafloor spreading during the last 5 Ma (Girdler and Styles 1974; Roeser 1975; LaBreque and Zitellini 1985; Ghebreab 1998). The seismicity of the central and southern Red Sea areas are mainly confined to the deep, axial trough where there are north north east (NNE) transform faults (Fairhead and Girdler 1970). The southern part of the Red Sea had long-term moderate to high levels of seismicity, which can be associated with volcanism which has been observed in Yemen and Ethiopia (Ambraseys et al. 1995).

Unlike the central and southern parts, the northern part of the Red Sea has had a remarkably large number of earthquakes with low and moderate magnitudes on the Richter scale during the period from 1990 to 2009. A cluster is located in an area of late stage, continental rifting, which is comprised of a broad trough without a recognizable spreading center, although there are a number of small isolated deep troughs (Ghebreab 1998). According to Al-Amri (1995), the low level of seismic activity in the northern part of the Red Sea compared with the southern Red Sea and the Gulf of Aqabah may be due to: (1) the occurrence of low-magnitude earthquakes that occur in the region but do not transmit enough energy to be recorded on distant stations and/or (2) lithospheric deformations in this region are occurring on land rather than under the sea. According to Hamouda (2009), this area has been considered to have significant moderate levels of magnitude earthquake activity which may be due to its complicated tectonic structures and to the relative motion at the triple junction between the African plate, the Arabian plate, and the Sinai subplate (Bosworth and Taviani 1996; Dahy 2010).

Conclusions

The result show that (1) the pattern analysis techniques applied to the seismic data catalog of earthquakes beneath the Red Sea can detect clusters in the occurrence of earthquakes from 1900 to 2009; (2) the spatial pattern of earthquakes with higher magnitudes on the Richter scale were notably concentrated in the central and southern parts of the Red Sea, while a remarkably high number of earthquakes with low and moderate magnitudes on the Richter scale occurred in the northern part of the Red Sea; (3) spatial statistical analysis can be a valuable method for showing complex spatial phenomena such as clusters of earthquakes and spatial patterns between locations and seismic, tectonic, and other processes. The authors were fortunate in having access to an earthquake data catalog covering a period from 1900 to 2009 for use in this study. Given the advances in electronic and communication technologies in recent years and in the design, production, and sensitivity of multichannel seismic field recorders, much more detailed seismic data should be captured over an even greater geographical area in order to provide a richer dataset for analysis using the methods outlined in this paper.

References

Abdel-Rahman K, Al-Amri A, Abdel-Mneim E (2009) Seismicity of Sinai Peninsula, Egypt. Arab J Geosci 2:103–118

Al-Amri A (1995) Recent seismic activity in the northern Red Sea. J Geodyn 20(3):243–253

Al-Amri A, Punsalan BT, LJy EA (1998) Spatial distribution of the seismicity parameters in the Red Sea regions. J Asia Earth Sci 16(5–6):557–563

Al-Tarazi E (2000) The major Gulf of the Aqaba earthquake, 22 November 1995—maximum intensity distribution. Nat Hazard 22:17–27

Ambraseys NN, Adams RD, Melville CP (1995) The seismicity of Egypt, Arabia and the Red Sea: a historical review. Cambridge University Press, Cambridge

Anselin L (1995) Local indicators of spatial association—LISA. Geogr Anal 27:93–115

Anselin L (2005) Exploring spatial data with GeoDATM: a workbook. Spat Anal Lab 138

Bailey TC, Gatrell AC (1995) Interactive spatial data analysis. Wiley, New York, NY

Bonatti E (1985) Punctiform initiation of sea-floor spreading in the Red Sea during transition from a continental to oceanic rift. Nature 316:33–37

Bosworth W, Taviani M (1996) Late Quaternary reorientation of stress field and extension direction in the southern Gulf of Suez, Egypt: evidence from uplifted coral terraces, mesoscopic fault arrays, and borehole breakouts. Tectonics 15:791–802

Choy GL, Kind R (1987) Rupture complexity of a moderate-sized (mb6.0) earthquake: broad band body wave analysis of the North Yemen earthquake of 13 December 1982. Bull Seismol Soc Am 77(1):28–46

Cochran JR (1983) Model for development of the Red Sea. Am Assoc Pet Geol Bull 67:41–69

Cochran JR, Martinez F, Steckler MA, Hobart MA (1985) The northern Red Sea, pre-sea-floor tectonics. EOS Trans AGU 66:365

Cochran JR, Martinez F, Steckler MA, Hobart MA (1986) Conrad Deep, a new northern Red Sea deep, origin and implications for continental rifting. Earth Planet Sci Lett 78:18–32

Dahy SA (2010) A study on seismicity and tectonic setting in the northeastern part of Egypt. Res J Earth Sci 2(1):8–13

Diggle PJ (2003) Statistical analysis of spatial point patterns, 2nd edn. Arnold, London

El-Shazly EM (1982) The Red Sea region. In: Nairs AEM, Stehli FG (eds) The oceans basins margins, the Indian ocean, vol. 6. Plenum, New York, pp 205–252

Faenza L, Marzocchi W, Lombardi AM, Console R (2004) Some insights into the time clustering of large earthquakes in Italy. Ann Geophys 47(5):1635–1640

Fairhead JD, Girdler RW (1970) The seismicity of the Red Sea, Gulf of Aden and Afar Triangle. Phil Trans Roy Soc London A 267:49–74

Fotheringham AS, Brunsdon C, Charlton ME (2002) Geographically weighted regression: the analysis of spatially varying relationships. Wiley, Chichester

Gardner JK, Knopo L (1974) Is the sequence of earthquakes in Southern California, with aftershocks removed, Poissonian? Bull Seismol Soc Am 64(5):1363–1367

Getis A, Ord JK (1992) The analysis of spatial association by use of distance statistics. Geogr Anal 24:189–206

Ghebreab W (1998) Tectonics of the Red Sea region reassessed. Earth Sci Rev 45:1–44

Girdler RW, Styles P (1974) Two stage sea-floor spreading. Nature 247:7–11

Hamouda AZ (2009) Assessment of seismic hazards for Hurghada, Red Sea, Egypt. Nat Hazards 59:465–479

Han S, Ishioka F, Kurihara K (2008) Detection of hotspot for Korea earthquake data using echelon analysis and seismic wave energy. J Fac Environ Sci Technol 13(1):51–56

Holden L, Sannan S, Bungum H (2003) A stochastic marked point process model for earthquakes. Nat Hazards Earth Syst Sci 3:95–101

Kalkhan M (2011) Spatial statistics: geospatial information modeling and thematic mapping, 1st edn. CRC Press, New York

Kim TG, Yi T, Lee E, Ryu HW, Cho K (2012) Characterization of a methane-oxidizing biofilm using microarray, and confocal microscopy with image and geostatic analyses. Appl Microbiol Biot 95:1051–1059

Korrat IM, Hussein HM, Marzouk I, Ibrahim EM, Abdel-Fattah R, Hurukawa N (2006) Seismicity of the northernmost part of the Red Sea (1995–1999). Acta Geophys 54(1):33–49

LaBreque JL, Zitellini N (1985) Continuous sea-floor spreading in Red Sea, an alternative interpretation of magnetic anomaly pattern. Bull Am Assoc Pet Geol 69:513–524

McKenzie DP, Davies D, Molnar P (1970) Plate tectonics of the Red Sea and East Africa. Nature 226:242–248

Mitchell A (1999) The ESRI guide to GIS analysis, geographic patterns and relationships. ESRI, Redlands, CA

Mitchell A (2005) The ESRI guide to GIS analysis, spatial measurements and statistics. ESRI, Redlands, CA

Musmeci F, Vere-Jones D (1992) A space–time clustering model for historical earthquakes. Ann Inst Stat Math 44(1):1–11

Ogata Y (1988) Statistical models for earthquake occurrences and residual analysis for point processes. J Am Stat Assoc 83(401):9–27

Ord JK, Getis A (1995) Local spatial autocorrelation statistics: distributional issues and an application. Geogr Anal 27(4):286–306

Páez A (2004) Anisotropic variance functions in geographically weighted regression models. Geogr Anal 36(4):299–314

Pautot G, Bourgois J, Bandy W, Boinet T, Chotin P, Huchon P, Mercier de Lepinay B, Monge F, Monlau J, Pelletier B, Sosson M, von Huene R (1986) Fragmentation of the Nazca Plate west of the Peru Trench: results of the R.V. Jean-Charcot SEAPERC cruise. C R Acad Sci Paris 303:1651–1656 (in French with English abstract)

Pei T (2011) A nonparametric index for determining the numbers of events in clusters. Math Geosci 43:345–362

Pei T, Zhua AX, Zhou C, Li B, Qin C (2007) Delineation of support domain of feature in the presence of noise. Comput Geosci 33:952–965

Pei T, Zhu A-X, Zhou C, Li B, Qin C (2009) Detecting feature from spatial point processes using collective nearest neighbor. Comput Environ Urban 33(6):435–447

Roeser HA (1975) A detailed magnetic survey of the southern Red Sea. Geol Jahrb D-13:131–153

Scott LM, Janikas MV (2010) Spatial statistics in ArcGIS. In M.M. Fischer and A. Getis (eds.). Handbook of applied spatial analysis: 27 software tools, methods and applications

Shurygin AM (1993) Statistical analysis and long-term prediction of seismicity for linear zones. Math Geol 25(7):759–772

Silverman BW (1986) Density estimation for statistics and data analysis. Chapman Hall, London, UK

Vasudevan K, Eckel S, Fleischer F, Schmidt V, Cook FA (2007) Statistical analysis of spatial point patterns on deep seismic reflection data: a preliminary test. Geophys J Int 171(2): 823–840

Vere-Jones D (1970) Stochastic models for earthquake occurrence (with discussion). J R Stat Soc Ser B 32(1):1–62

Vere-Jones D, Deng YL (1988) A point process analysis of historical earthquakes from North China. Earthquake Research in China (Chung-kuo tic hen yen chiu), 4: 8–19 (in Chinese). English translation: Earthquake Res in China, 2:165–181

Xie Z, Yan J (2008) Kernel density estimation of traffic accidents in a network space. J Comput Environ Urban Syst 32:396–406

Zimeras S (2008) Exploratory point pattern analysis for modeling earthquake data. 1st WSEAS Int Conf Environ Sci Eng (EG'08), Malta